Methyl Selenol as Precursor in Selenite Reduction to Se/S Species by Methane-oxidizing Bacteria.

ESWAYAH, Abdurrahman S., HONDOW, Nicole, SCHEINOST, Andreas C., MERROUN, Mohamed, ROMERO-GONZÁLEZ, Maria, SMITH, Thomas J. <http://orcid.org/0000-0002-4246-5020> and GARDINER, Philip H.E. <http://orcid.org/0000-0002-2687-0106>

Published version

ESWAYAH, Abdurrahman S., HONDOW, Nicole, SCHEINOST, Andreas C., MERROUN, Mohamed, ROMERO-GONZÁLEZ, Maria, SMITH, Thomas J. and GARDINER, Philip H.E. (2019). Methyl Selenol as Precursor in Selenite Reduction to Se/S Species by Methane-oxidizing Bacteria. Appl Environ Microbiol.

Copyright and re-use policy

Methyl Selenol as Precursor in Selenite Reduction to Se/S Species by Methane-oxidizing Bacteria

Methyl Selenol as Precursor in Selenite Reduction

Abdurrahman S. Eswayah[1,2], Nicole Hondow[3], Andreas C. Scheinost[4], Mohamed Merroun[5], Maria Romero-González[6], Thomas J. Smith[1] and Philip H. E. Gardiner[1#]

[1]*Biomolecular Sciences Research Centre, Sheffield Hallam University, Sheffield, UK*

[2]*Biotechnology Research Centre, Tripoli, Libya*

[3] *School of Chemical and Process Engineering, University of Leeds, Leeds, UK*

[4]*The Rossendorf Beamline at ESRF, F-38043 Grenoble, France, and Institute of Resource Ecology, Helmholtz Zentrum Dresden Rossendorf, D-01328 Dresden*

[5]*Department of Microbiology, University of Granada, Granada, Spain*

[6] *School of Engineering and Materials Science (SEMS), Queen Mary University of London, Mile End Road, London E1 4NS.*

#To whom correspondence should be addressed: Biomolecular Sciences Research Centre, Sheffield Hallam University, Sheffield, S11WB, UK.

E-mail: p.h.gardiner@shu.ac.uk

Abstract

A wide range of microorganisms have been shown to transform selenium-containing oxyanions to reduced forms of the element, particularly selenium-containing nanoparticles. Such reactions are promising for detoxification of environmental contamination and production of valuable selenium-containing products such as nanoparticles for application in biotechnology. It has previously been shown that aerobic methane-oxidising bacteria, including *Methylococcus capsulatus* (Bath), are able to perform methane-driven conversion of selenite (SeO_3^{2-}) to selenium-containing nanoparticles and methylated selenium species.

Here, the biotransformation of selenite by *Mc. capsulatus* (Bath) has been studied in detail via a range of imaging, chromatographic and spectroscopic techniques. The results indicate that the nanoparticles are produced extracellularly and have a composition distinct from nanoparticles previously observed from other organisms. The spectroscopic data from the methanotroph-derived nanoparticles are best accounted for by a bulk structure composed primarily of octameric rings in the form $Se_{8-x}S_x$ with an outer coat of cell-derived biomacromolecules. Among a range of volatile methylated selenium and selenium-sulfur species detected, methyl selenol (CH_3SeH) was found only when selenite was the starting material, although selenium nanoparticles (both biogenic and chemically produced) could be transformed into other methylated selenium species. This result is consistent with methyl selenol being an intermediate in methanotroph-mediated biotransformation of selenium to all the methylated and particulate products observed.

Importance

Aerobic methane-oxidizing bacteria are ubiquitous in the environment. Two well characterised strains, *Mc. capsulatus* (Bath) and *Methylosinus trichosporium* OB3b, representing gamma- and alpha-proteobacterial methanotrophs, can convert selenite, an environmental pollutant, to volatile selenium compounds and selenium containing particulates. Both conversions can be harnessed for bioremediation of selenium pollution using biological or fossil methane as the feedstock and these organisms could be used to produce selenium-containing particles for food, and biotechnological applications. Using an extensive suite of techniques we identified precursors of selenium nanoparticle formation, and also that these nanoparticles are made up of eight membered mixed selenium and sulfur rings.

Keywords: Selenite reduction, Elemental selenium, Methane-oxidizing bacteria, Mixed chalcogenide amorphous nanoparticles

Introduction

A key biotransformation mechanism of most microorganisms exposed to selenium oxyanions is dissimilatory reduction to nanoparticulate elemental selenium (1-4). The formation of the nanoparticles (NPs) reduces the toxicity and bioavailability of the selenium species (5-9). Not only does the formation of the NPs reduce the adverse environmental impact of the oxyanions on the microorganisms and their surroundings they also present an approach for the production of selenium NPs designed for a variety of technological, clinical, analytical and industrial applications (10-20). There is a demand for nanoparticles with new combinations of properties for specific applications. In the case of selenium-containing particles, to date these have included exploitation of their optical properties to improve the response of sensors (11), binding of heavy metal ions to effect remediation of pollution (12) and exploitation of the antitumour (16), immunomodulatory (17) and antimicrobial (19) activities of specific types of selenium-containing particles.

Different bacteria are known to convert selenium oxyanions into red amorphous Se NPs with distinct features. Selenium NPs produced by the selenium-respiring bacteria *Sulfurospirillum barnesii* and *Bacillus selenitireducens* contain predominantly Se_6 chain units, while *Selenihalanaerobacter shriftii* has Se_8 rings (21). *Desulfovibrio desufuricans,* a sulfate-reducing bacterium, produces amorphous spherical submicro particles containing selenium and sulfur (22). Selenium NPs produced from selenite by *Azospirillum brasilense* are composed of cyclic $Se_{8-x}S_x$, with Se_6S_2 the most likely structure (8). *Azospirillum thiophilum* produce amorphous selenium particles with no evidence of either Se-S or S-S bands in the

Raman spectrum (23). *Stenotrophomonas bentonitica* produces amorphous Se^0 nanospheres that subsequently transformation to one-dimensional (1D) trigonal selenium nanostructure where sulfur is associated with the SeNPs (24). In an earlier study, (25), we presented indirect evidence from transmission electron microscopy (TEM) imaging with energy dispersive X-ray spectrometry (EDX) measurements to show that sulfur was associated with amorphous selenium in the extracellular NPs that are produced in a methane-dependent fashion from the reduction of selenite by the aerobic obligate methane-oxidizing bacteria *Methylococcus capsulatus* (Bath) and *Methylosinus trichosporium* OB3b.

Besides the above-mentioned studies on the biotransformation of selenium oxyanions most investigations have focused on the formation of the NPs. A few others have identified concomitant release of volatile selenium species into the headspace gas (26, 27). However, none of these approaches has provided enough information to enable the elucidation of the processes leading to the formation of the amorphous NPs. Indeed, the formation of the extracellular amorphous NPs forms as reported in many studies (18, 21, 28-30) may indicate limited direct involvement of the microorganisms in their formation, although the initial reactants may have been produced in the bacteria. The size of the extracellular nanoparticles produced by *Mc. capsulatus* Bath increased with time (25), which suggested that the growth of the NPs is a result of abiotic reactions in the culture medium outside the cells. The formation of mixed chalcogenide species by exchange reactions, when both Se and S species are present in the gaseous and solution phase, has been reported (31, 32). It is probable that similar reactions occur in the culture medium solution resulting eventually to the formation of the nanoparticles. Here, it was our intention to observe the process of nanoparticle formation and structure of the nanoparticles in greater detail and to be better able to understand the biotic and abiotic transformations occurring in the methanotroph-mediated transformation of selenite. To this end, both selenium- and sulfur-containing species were sampled from the

headspace and solution of selenite amended and control samples at fixed times by sorptive extraction in conjunction with analysis by thermal desorption - gas chromatography- mass spectrometry (TD-GC-MS) to identify the compounds. In parallel, the formed NPs were characterised by a range of physical techniques, namely; attenuated total reflectance Fourier transformation infrared spectroscopy (ATR-FTIR), Raman spectroscopy, transmission electron microscopy (TEM) and energy dispersive X-ray (EDX) spectrometry, X-ray absorption spectroscopy (XAS), and X-ray photoelectron spectroscopy (XPS). Herein, the results obtained from these measurements are used to inform the formation and elucidation of the structure of the sulfur-doped red amorphous selenium NPs produced when a methane-oxidizing bacterium reduces selenite. *Mc. capsulatus* (Bath) was chosen for these experiments since it transforms selenite at approximately five times the rate of *Ms. trichosporium* OB3b (25).

Results

Previous investigations with the methanotroph species *Mc.capsulatus* (Bath) showed that the sizes of the NPs grew rapidly from an average of 220 ±51 nm in the first 4 hrs to about 400 ±77 nm in the next 44 hrs as previously published (25). Here, high angle annular dark field-scanning transmission electron microscopy (HAADF-STEM) imaging and TEM thin-section micrographs of cultures producing the nanoparticles were performed and it appears that the NPs are associated extracellularly with the cells (see Fig. 1a). Furthermore, the spatial distributions of Se and S in the EDX maps overlap, indicative of a spatial and likely structural association, suggesting the formation of mixed chalcogenide nanoparticles (see Fig.1b). The intensity of the Se signals was, however, much higher than that for S (see Fig. 1c). In addition, examination of the $S_{k\alpha}$ map (Fig. 1b) reveals that not only was there sulfur in the particles but

there was a “trail” of the element linking the particles to the cells, suggesting likely sulfur-containing proteins from the bacterial cells.

Se K-edge X-ray Absorption Near-Edge Structure (XANES) spectra of the particles formed by *Mc. capsulatus* (not shown) are similar to those of red amorphous Se with no detectable residual selenite present in the samples. Previous shell fitting of the Extended X-ray Absorption Fine-Structure (EXAFS) spectra formed by *Mc. capsulatus* (25) showed the characteristics of amorphous elemental Se^0, with two atoms at a distance of 2.35Å, however this is slightly shorter than 2.36Å expected for red elemental Se (33,34). The shorter bond length is an indication that there may be partial substitution of Se for the smaller S atom in the structure of the amorphous red elemental Se. This is a feature that has been observed for mixed Se and S nanoparticles formed by *A. brasilense* (35). In order to unravel the make-up of the nanoparticles, the surfaces of the particles were characterized by FTIR, XPS and Raman spectroscopy.

FTIR Analysis

The FTIR spectra of the freeze-dried selenium nanoparticles produced by the *Mc. capsulatus* in liquid NMS medium amended with selenite, the Chem-SeNPs (in-house produced selenium nanoparticles as described in the experimental section) and the bacterial biomass are shown in Figure 2. The assignments of the bands, which are based upon the characteristic vibrational frequencies of the different types of covalently bonded atoms, are summarised in Table 1. The peak centred at 3297 cm^{-1} corresponds to the −OH and −NH stretching vibrations of the amine and carboxylic groups. Peaks at 2927 cm^{-1} corresponded to the aliphatic saturated C−H stretching modes (30, 36). The peaks at 1644, 1538, and 1239 cm^{-1} are characteristic of amide I, amide II, and amide III bands of proteins, respectively (37, 38). The symmetrical stretch of carboxylate group can be attributed to the bands observed at 1366

144 cm^{-1}. The peaks at 1150, 1077 and 1015 cm^{-1} corresponded to the C−O stretching vibrations
145 of C-O-C groups (37, 39). The presence of phosphoryl groups was confirmed by the peak at
146 929 cm^{-1}. Additionally, peaks at 859 and 762 cm^{-1} (fingerprint region) could be mainly
147 attributed to aromatic ring vibrations of aromatic amino acids (tyrosine, tryptophan,
148 phenylalanine) and possibly nucleotides (40, 41).

149 The FTIR spectra of SeNPs of *Mc. capsulatus* differ from those of the bacterial biomass
150 (control) and the Chem-SeNPs. The main difference between the spectra is that the Bio-
151 SeNPs exhibit more peaks in the protein and polysaccharide vibration region, indicating the
152 presence of proteins and polysaccharides in the biomacromolecules capping the SeNPs (20,
153 30, 42, 43).

154 By contrast, Chem-SeNPs obtained through reaction of Na_2SeO_3 with L-cysteine displayed a
155 broad absorption band around 3350 cm^{-1} and absorption band at 2923 cm^{-1} that are assigned
156 to O−H vibrations of the absorbed H_2O and C−H vibration in the alkyl chain of L-Cys,
157 respectively. The peak at 1606 cm^{-1}can be mainly attributed to C=O vibrations. It is
158 noteworthy that the presence of organic residues such as carbohydrates, lipids, and proteins
159 on the surface of biogenic SeNPs were completely absent in the Chem-SeNPs spectrum (see
160 Figure 2). FTIR spectra of the Bio-SeNPs separated from the *Mc. capsulatus* cells showed
161 bands typical of proteins, polysaccharides and lipids associated with the particles.

162 **XPS analysis of the particle surface**

163 The surface composition of the harvested red particles was obtained by XPS, which is a
164 surface technique that obtains information about the elemental composition of a sample
165 according to the emission of photoelectrons when the sample is irradiated with X-ray energy.
166 The signals observed in XPS can be identified based on their binding energy as arising from
167 expulsion of electrons from specific energy levels within each element on the surface (rather

than the interior) of the particles. Hence, the surface elemental content can be summarised from the full range XPS spectrum (Supplemental Figure 1a). In addition to the selenium which is present at a concentration of 1.25% (atomic percent), there are five other elements: carbon (46.32%), oxygen (31.41%), nitrogen (8.61%), calcium (5.89%) and phosphorus (4.77%) that were detected on the surface of the particles (see Supplemental Figure 1a and the elemental information therein). The presence of the first three elements is an indication that there are organic molecules on the particle surfaces. The high resolution spectral scans, which show the regions due, respectively, to Se, C, N, and O, and the assigned chemical species from the core level XPS spectra of C1s, N 1s, O 1s bands are shown in Figures 3b-e. These spectra are consistent with the presence of biomolecules, including proteins, on the surface of the particles. The spectrum for 3d Se shows a doublet which does not show base-line resolution. However, the fitted deconvoluted peaks in this region (Supplemental Figure 1b) show two predominant bands at 55.16 and 56.02 binding energy (eV), and two minor peaks at 55.75 and 56.61 eV, respectively, the latter pair of peaks resulting from the Se 3d peak split by spin orbit coupling into Se 3d5/2 and Se 3d3/2. The key conclusion enabled by these results is that the observed range of binding energies between 55.16 and 56.61eV is indicative of the presence of reduced selenium species, including elemental selenium at the surface of the particles (44). The binding energy expected for the Se 3d electrons in selenite (SeO_3^{2-}) is indicated in Supplemental Figure 1b; it is clear that no signal at this position is observed.

Raman characterisation of the amorphous particles

Vibrational spectroscopy particularly Raman spectroscopy (which is a visible light scattering technique that gives information complementary to that from IR spectroscopy) has been the technique of choice for the characterization of Se_n allotropes, and aggregates. The deconvoluted Raman spectrum obtained between 50-600 cm^{-1} shows the shift in frequency of

193 the scattered light that corresponds to the vibrational spectrum of the harvested SeNPs
194 (Figure 3). There are four bands which are visible: the main band at 251.5 cm^{-1} and smaller
195 ones at 80.2, 358.8 and 506.5 cm^{-1}, respectively. All of the bands were present in all of the
196 scans of samples collected at different time points: 6, 24 (supplemental Figure 2) and 48 h
197 (Figure 3). The band at 506.5 cm^{-1} was more prominent than that at 358.8 cm^{-1}. The band at
198 80.2 cm^{-1}, which is a shoulder, is only visible in the deconvoluted spectrum.

199 It has been proposed that amorphous selenium is composed of a mixture of Se_n rings and
200 helicoidal chains (45-47). The proportion of each depends on chemical and physical
201 conditions under which the samples are made, and the treatments to which they have been
202 subjected. According to Carini et al the band at around 250 cm^{-1} is characteristic of
203 amorphous selenium (48). The symmetrical band at 251.5 cm^{-1}, with full width half maxima
204 of 30 cm^{-1} found in this study, is characteristic of Se-Se stretching vibration in pure Se_8 (45,
205 49, 50) with its deformation vibration at 80.2 cm^{-1}. However, in the study of mixed selenium
206 and sulfur alloys by Machado et al, the authors state that as the sulfur concentration increases
207 in mixed amorphous selenium, the peak at 234 cm^{-1} usually associated with Se chains
208 decreases in intensity and the band at 250 cm^{-1}, usually associated with selenium rings
209 increases in intensity. They also observed the appearance of a band at 352 cm^{-1} as the
210 selenium to sulfur ratio increases to either 4:1 or 7:3 (51). The band at 358.8 cm^{-1} has been
211 assigned to S-Se stretching vibration (52, 53). The band at 506.5 cm^{-1} is probably due to the
212 Se-Se overtone band of the fundamental band at 251.5 cm^{-1}. The S-S vibration band is not
213 seen when the S composition is below that found in Se_6S_2 (45). Therefore it is probable that
214 the composition of the harvested particles is Se_{8-x}, S_x , where x is equal to or greater than 2.

215

216

Speciation of selenium and sulfur in the medium solution and headspace

The GC-MS chromatograms of the species found in both the headspace and solution of the selenite amended medium at 4h and 20h are shown in Supplemental Figure 3. The earlier time was chosen because the formation of the particles and therefore the red colour of the solution were barely discernible. A summary of the selenium- and sulfur-containing species is given in Table 2. Examination of the data in Table 2 showed that after 4 h, three compounds: methyl selenol (CH_3SeH), dimethyl selenenyl sulfide (DMSeS; CH_3-Se-S-CH_3) and dimethyl diselenide (DMDSe; CH_3-Se-Se-CH_3) were detected in both the solution and headspace. In addition dimethyl diselenenyl sulfide (CH_3-Se_2S-CH_3) and Bis(methylseleno) methane (CH_3-Se-CH_2-Se-CH_3) were also found in the solution. At 20 h, dimethyl selenenyl disulfide (CH_3-SeS_2-CH_3)was detected in the solution in addition to triselenothone/ dimethyltriselenide (CH_3-Se-Se-Se-CH_3) which was detected in both the solution and headspace. The control in the absence of selenite showed no selenium-containing species, though three sulfur-containing species were observed (Table 2).

Discussion

The results from the previous kinetic experiments showed that there were increases in particles sizes with incubation time (25) leading us to hypothesize that much of the structure of the particles was formed in the extracellular space. If data support this hypothesis, then the key reactions resulting in the increase in the particle sizes are essentially abiotic in nature, though they require electrons ultimately derived from methane. Consequently, the clues to the structural formation of the particles must lie in the nature and identity of the compounds that are concomitant in the solution and headspace of the nascent particles. It was therefore essential to sample for selenium- and sulfur-containing compounds in both the headspace and solution, followed by their analyses and identification.

The FTIR spectra of the SeNPs produced by *Mc. capsulatus*, samples of biomass of the strain (control), as well as the Chem-SeNPs were recorded in order to identify the functional groups capping the synthesized SeNPs. These results were consistent with the particles being coated with cell-derived proteins and other biomolecules and are in line with their TEM images showing a thin layer over the particles, in addition to strong carboxylate bands, which may stabilize the SeNPs structure and morphology.

The XPS results show two Se containing species, and other organic constituents. In assigning the Se bands, it is essential to link the structure of the particles to the selenium-containing species that have been identified in the solution (see the discussion of the TD-GC-MS results below). Since data for the exact compounds are not available, structures that may be similar to these in the particles have been selected. The major band at 55.16 eV, has been assigned to the compound: $(CH_3)_2NC(Se)SeC(Se)N(CH_3)_2$ (54). This is a reasonable fit to the results obtained in this study not only because of the presence of selenium but also the content of the methyl groups and nitrogen. The nitrogen could account for the single band at 400.10eV usually assigned to amine nitrogen. The bands at 56.02 eV has been assigned to (-$CSeC(CH_3)C(CH_3)Se$-)2 (55). Both of these assignments are an indication of the presence of long chain of selenium-containing methylated species. Missing from both spectra is oxygen which is presumably present as C=O, and either C-O-C or C-O-H at 531.58 and 532.84 eV, respectively. However, the presence of Se-C was not detected in the spectrum thus indicating the amount of carbon directly bound to selenium was low. Furthermore, because of the high concentration of selenium in relation to sulfur, the signal for the latter could not be resolved and identified.

Whereas, both FTIR and XPS provided information on the forms in which the elements are present on the particle surface, Raman spectroscopy enables the identification of the basic structural make-up of the particles. The intensity of the band 251.5 cm^{-1} is indicative of the

predominance of the Se-Se bonds in the structure of the particles. It is probable that S is integral to the mixed particle structure $Se_{8-x}S_x$, and not as an S_8 impurity in the particles. The low available sulfur content in the medium makes the formation of an S-S homonuclear bond in the mixed particle structure highly unlikely (52).

We have previously reported that methyl selenol is produced and detected in the head space only when selenite is in the starting medium (25). Methylated selenium-containing volatiles are known to be produced during transformation of selenium-containing species by other types of bacteria (reviewed in [5]), but the presence of methyl selenol has not been reported and may be unique to methanotrophs. Besides the presence of methyl selenol in the headspace, methyl selenoacetate was also detected. However, in the present study methyl selenoacetate was not detected when the headspace sorptive extraction probes were deployed for sample collection. No methyl selenol was detected when either the harvested or chemically synthesized nanoparticles were added to the medium in the absence of selenite. Therefore, we propose that methyl selenol may be the precursor of all of the methylated selenium species as well as the selenium-containing nanoparticles. If this is the case, the first step in the biotransformation of selenite by *Mc. capsulatus* would involve the reduction and methylation of selenite to methyl selenol followed by the formation of the other selenium- and sulfur-containing species. Indeed, the formation of some of the latter species requires the presence of the nascent selenium particles.

Based on these observations a possible pathway for the formation of the particles and the other products of biotransformation of selenite can be outlined as in Figure 4. A series of reactions proposed by Ganther (56, 57) and outlined by Xu and Barton (22) implicate glutathione (GSH) and GSH reductase in the production of elemental selenium. This is possible in *Mc. capsulatus*, in which glutathione is known (58), though would not account for possible differences in pathway from other microorganisms in which GSH and GSH

reductase are widespread. The proposed steps leading up to the formation of methyl selenol involving GSH is shown in Figure 5. Whilst the transformation of selenite by whole cells in culture requires the presence of the growth substrate methane, previous work showed that selenite was transformed by concentrated cell fractions (cell walls, membranes and the soluble fraction) to the red particulate material in the absence of methane. The fact that the greatest activity was found in the cell wall-enriched fraction (25) is consistent with the extracellular growth of the particles.

The presence of the sulfur-containing benzothiazole was detected, whether or not the culture had been amended with selenite. The sulfur-containing volatile species dodecanethiol and propanesulfonyl were detected only in the control cultures without selenite (Table 2). Such sulfur-containing species may be the source of sulfur in the structure of the selenium-rich particles. Evidence of the formation of the longer chains of the selenium- containing species can be seen in the nature of the compounds that are found in the solution after hours of incubation, first after 4h, dimethyl diselenenyl sulfide was detected, and subsequently dimethylselenodisulfide, dimethyltriselenide and bis(methylseleno) methane were detected after 20h. More complex mixed Se and S compounds are formed in the medium with time. The formation of the mixed chalcogenides of Se and S is hardly surprising since S may be available from the reduction of sulfate in the growth medium. Genes for assimilatory uptake and reduction of sulfate are present within the *Mc. capsulatus* genome (59) and the strain grows using sulfate as sole sulfur source. A key question therefore is how the solution chemistry relates to the observed structural features of the Se particulates.

It is likely that these longer chains polymerize to form Se_x or $Se_{8-x}S_x$ linear or cyclic structures (32). Indeed, all chalogen elements have the tendency to form cyclic allotropes (60). The dominant allotrope will depend on the experimental conditions. Examples of

exchange reactions that may occur based on the presence of the detected selenium- and sulfur- containing species are shown in the following equations:

-Se-Se- + 2-Se-Se-Se- ----->Se_8 (1)

-Se-S- + 2-Se-Se-Se- -----> Se_7S (2)

2-Se-Se-S- + -Se-Se- -----> Se_6S_2 (3)

As can be seen a variety of nanocomposites can be formed. It is noteworthy that these structures are methylated providing an organic coating associated with the nanoparticles (61) Similar exchange reactions have been shown to occur when mixed Se and S complexes are present in the same solution (32). Indeed these reactions are known to occur in amorphous selenium semiconductors (62). The Raman results indicate these are not open chain clusters but cyclic structures with the Se_8 structure dominant and the probable presence of small amounts of Se-S bonds. The source of sulfur must be from the reduction of sulfate used in the growth medium since this is the only sulfur added to the system. If it were desired to reduce the sulfur content of the particles, it may be possible to achieve this by reducing the amount of sulfate in the culture medium so that sulfur becomes growth-limiting. Since it may be that the cells can produce the nanoparticles after they have ceased to grow, this may allow the selenite to be added to the medium after the sulfate is used up, so that less sulfur would be available for incorporation into the particles.

In this study, we demonstrate for the first time that in the reduction of selenite by *Mc. capsulatus* (Bath), a methane oxidizing bacterium, methyl selenol is the likely precursor for the formation of methylated selenium-containing and mixed chalcogenides species. This reaction may be biotechnologically useful for bioremediation of selenite and production of selenium-sulfur nanoparticles for electronics and other applications, using cheaply available

methane as the feedstock. If this reaction is widespread among methanotrophs, it may also have significance in selenium transformations in the environment. To date, it has been shown that four isolated strains, including methanotrophs of the gammaproteobacteria (*Mc. capsulatus* Bath, *Mm. buryatense* and *Mm. alkaliphilum*) and alphaproteobacteria (*Ms. trichosporium* OB3b) perform this reaction.

Subsequent exchange reactions between the species result in the formation of the amorphous allotropic form of selenium, cyclic Se_8 with sulfur in its structure. The nature of the molecular mediators in reduction of selenite, supplying sulfur that is integral to the structure of the nanoparticles and supplying the methyl groups found in the volatile selenium containing products remain to be identified.

Materials and Methods

Bacterial strains and growth conditions

The methanotrophic bacterium *Methylococcus capsulatus* (Bath) (NCIBM 11132) was grown and propagated aerobically using methane as the carbon and energy source as previously described (25). For these experiments the initial selenite concentration used was 20 mg L^{-1}.

Detection of solution and volatile selenium species

Solution and volatile selenium-containing species were sampled by immersive sorptive extraction using sampling probes (HiSorb probe, Markes International, UK) from either the solution or headspace. Extension screw-on arms were fabricated for each probe so that they could be inserted through the Suba-Seals used to seal the necks of the culture flasks. To ensure that the probes and tubes were contamination free, before use, the probes and tubes were preconditioned with helium at flow rate of 90 mL min^{-1} using the following temperature programme: 15 min at 100 °C, 15 min at 200 °C, 15 min at 300 °C and 15 min at 335 °C.

The preconditioned probes were inserted into either the liquid or headspace of the *Mc. capsulatus* (Bath) culture medium through the Suba-Seals. The probes were removed from the Suba-Seals after different incubation time (4 and 20 h, respectively), rinsed with HPLC grade water, dried with lint-free tissue, and then placed into the thermal desorption tubes (Markes International, UK).

Samples analyses were performed on a combined thermal desorption GC–MS system. The volatiles were desorbed at 250°C and concentrated on a thermal desorber (Unity®, Markes International Limited) at -10°C cold trap for 5 min (helium flow 50 mL min^{-1}) and then were transferred onto the GC/MS system (7890A-GC with 5975C-MS, Agilent Technologies) equipped with a capillary column (Agilent J&W HP-5MS GC Column, 30 m, 0.25 mm, 0.25 μm). Helium was used as the carrier gas at a flow rate of 1 mL min^{-1}, injector temperature, 250°C, and the chromatogram was obtained using the following temperature programme: 35°C for 1 min; 10°C min^{-1} to 250°C; and then held at 250°C for 1 min. The National Institute of Standards and Technology (NIST) MS search program (version 2011) was used to identify the compounds based on their MS spectrum.

Extraction of selenium nanoparticles produced by *Mc. capsulatus* (Bath)

Freshly grown cultures (at OD_{600} of 0.5-0.8) were supplemented with 20 mg L^{-1} SeO_3^{2-} and incubation was continued at 45°C with shaking in the presence of methane. After 48h the development of the reddish colour had occurred, the cultures were pelleted by centrifugation (at 12,500 × *g*; 10 min). SeNPs were extracted by a modification of the method published by Sonkusre et al. (63) , as follows. The resultant pellet was washed and re-suspended in 10 mL of sterile water followed by addition of lysozyme to give a final concentration of 500 μg mL^{-1} and the tube was incubated at 37°C for 3 h. The suspension was passed through a French pressure cell (1500 psi, 4°C). The resultant slurry containing both cell debris and NPs was washed four times at 15,000 × *g* for 10 min with 1.5 M Tris-HCl (pH 8.3) containing 1%

sodium dodecyl sulfate (SDS). The resultant pellet containing SeNPs and the insoluble cell wall fraction was washed and resuspended in 4 mL sterile water in a 15 mL Falcon tube, and 2 mL of 1-octanol were added. The solution was mixed vigorously on a vortex mixture for five min and centrifuged at 2000 × g for 5 min at 4°C. The tubes were then kept undisturbed at 4°C for 24 hours. The upper phase and interface containing the insoluble cell fraction were removed, and the bottom water phase containing SeNPs was transferred to a clean 15 mL centrifuge tube. This was washed sequentially with chloroform, absolute ethanol, 70% ethanol, and water at 16000 × *g*. Collected NPs were re-suspended in water and stored at 4°C.

Transmission electron microscopy (TEM) and energy dispersive X-ray (EDX) spectrometry/high-angle annular dark-field (HAADF) scanning TEM (STEM) analysis

Samples of selenite amended culture were treated and analysed as previously described (25). The samples were examined in an FEI Tecnai F20 field emission gun (FEG)-TEM operating at 200 kV and fitted with a Gatan Orius SC600A CCD camera, an Oxford Instruments XMax SDD EDX detector and a high-angle annular dark-field (HAADF) scanning TEM (STEM) detector.

For thin section analysis, after the ethanol dehydration steps, the cells were embedded in EM bed 812 epoxy resin and cut into thin sections (90 nm, using a diamond knife on a Reichert Ultracut S ultramicrotome). The sections were supported on copper grids and coated with carbon. TEM specimen holders were cleaned by plasma prior to TEM analysis to minimize contamination. Samples were examined with a high-resolution Philips CM 200 transmission electron microscope at an acceleration voltage of 200 kV under standard operating conditions with the liquid nitrogen anti-contaminator in place.

X-ray absorption spectroscopy

The conditions for the X-ray absorption spectroscopy measurements were as described previously (25).

X-ray photoelectron spectroscopy (XPS) analysis

Harvested SeNPs samples were deposited on silicon wafer, left to dehydrate in the load lock of the XPS instrument overnight. The analyses were carried out using a Kratos Axis Ultra DLD instrument with the monochromated aluminium source. Survey scans were collected between1200 to 0eV binding energy, at 160 eV pass energy and 1 eV intervals. High-resolution C 1s, N 1s, O 1s, Se 3d and S 2p spectra were collected over an appropriate energy range at 20 eV pass energy and 0.1 eV intervals. The analysis area was 700 μm by 300 μm. Two areas were analysed for each sample, collecting the data in duplicate. Charge neutralisation was used with intention of preventing excessive charging of the samples during analysis. The data collected were calibrated in intensity using a transmission function characteristic of the instrument (determined using software from NPL) to make the values instrument independent. The data were then be quantified using theoretical Schofield relative sensitivity factors. The data were calibrated for binding energy using the main carbon peak C 1s at 285.0 as the reference peak, and correcting all data for each sample analysis accordingly.

Raman spectroscopy analysis of SeNPs

Aliquots of 2 μL of SeNPs suspended in water were transferred onto a calcium fluoride (CaF_2) slide and air-dried prior to Raman analysis. Raman spectra were obtained using a Horiba LabRam HR and a modified Horiba LabRam HR (Wellsens Biotech. Ltd., China). Three factors have been modified in this new Raman system to improve Raman spectral quality. These comprise shortening the Raman light path, employing a low noise and sensitive EMCCD for the Raman signal detection, and increasing incident laser power. The old and new modified systems are identical except these three factors. The Raman signals were collected by a Newton EMCCD (DU970N-BV, Andor, UK) utilizing a 1600 × 200 array of 16 μm pixels with thermoelectric cooling down to −70°C for negligible dark current. A 532 nm Nd:YAG laser (Ventus, Laser Quantum Ltd., UK) was used as the light source for

Raman measurement. A 100× magnifying dry objective (NA = 0.90, Olympus, UK) was used for sample observation and Raman signal acquisition. A 600 line/mm grating was used for the measurements, resulting in a spectral resolution of ~1 cm^{-1} with 1581 data points. The laser power on sample was measured by a laser power meter (Coherent Ltd.). The Raman spectra were processed by background subtraction (using spectra from cell free region on the same slide) and normalization using the Labspec5 software (HORIBA Jobin Yvon Ltd., UK).

Fourier transformation infrared (FT-IR) spectroscopy measurements of SeNPs

In order to determine the functional groups present on the SeNPs, the FTIR spectra of SeNPs were recorded on a PerkinElmer Spectrum 100 FT-IR Spectrometer equipped with an attenuated total reflectance (ATR) attachment. Spectra were recorded from 4,000 to 650 cm^{-1}, and 4 scans were averaged at a resolution of 4 cm^{-1}. Extracted SeNPs were freeze dried overnight and analyzed without further treatment. For comparison, the FTIR spectra of samples of bacterial cells (as control) and chemically synthesized SeNPs (Chem-SeNPs) were also recorded. For the controls, freshly grown cultures (OD_{600} ~ 0.7) of *Mc. capsulatus* (Bath) were centrifuged at 11000 × *g* for 10 min to obtain the cell pellets. The pellets were washed twice with phosphate buffered saline (Sodium chloride, 150 mM, and sodium phosphate, 150 mM) pH 7.2, and then freeze dried overnight. The synthesis of Chem-SeNPs was done according to the procedure of (63) as follows: 1.0 mL of 50 mM L-cysteine (Sigma-Aldrich, Dorset, UK) solution was added dropwise into 1.0 mL of 0.1 M Na_2SeO_3. The mixed solution was then stirred for 30 min at room temperature. The Chem-SeNPs were pelleted by centrifugation (at 15000 × *g*; 10 min), and then freeze dried overnight.

Acknowledgement

ASE is grateful for the award of a PhD scholarship from the Ministry of Education, Government of Libya.

Conflict of Interest

The authors declare no conflict of interest.

References

1. **Kessi J, Ramuz M, Wehrli E, Spycher M, Bachofen R.** 1999. Reduction of selenite and detoxification of elemental selenium by the phototrophic bacterium *Rhodospirillum rubrum*. Appl Environ Microbiol **65:**4734-4740.

2. **Nancharaiah YV, Lens PN.** 2015. Ecology and biotechnology of selenium-respiring bacteria. Microbiol Mol Biol Rev **79:**61-80. doi:10.1128/MMBR.00037-14 [doi].

3. **Lortie L, Gould WD, Rajan S, McCready RG, Cheng KJ.** 1992. Reduction of slenate and slenite to eemental selenium by a *Pseudomonas stutzeri* Isolate. Appl Environ Microbiol **58:**4042-4044.

4. **Prakash NT, Sharma N, Prakash R, Raina KK, Fellowes J, Pearce CI, Lloyd JR, Pattrick RA.** 2009. Aerobic microbial manufacture of nanoscale selenium: exploiting nature's bio-nanomineralization potential. Biotechnol Lett **31:**1857-1862.

5. **Eswayah AS, Smith TJ, Gardiner PH.** 2016. Microbial Transformations of Selenium Species of Relevance to Bioremediation. Appl Environ Microbiol **82:**4848-4859. doi:10.1128/AEM.00877-16 [doi].

6. **Combs GF, Garbisu C, Yee BC, Yee A, Carlson DE, Smith NR, Magyarosy AC, Leighton T, Buchanan BB.** 1996. Bioavailability of selenium accumulated by selenite-reducing bacteria. Biol Trace Elem Res **52:**209-225.

7. **Song D, Li X, Cheng Y, Xiao X, Lu Z, Wang Y, Wang F.** 2017. Aerobic biogenesis of selenium nanoparticles by *Enterobacter cloacae* Z0206 as a consequence of fumarate reductase mediated selenite reduction. Scientific Reports **7:**3239.

8. **Vogel M, Fischer S, Maffert A, Hübner R, Scheinost A, Franzen C, Steudtner R.** 2018. Biotransformation and detoxification of selenite by microbial biogenesis of selenium-sulfur nanoparticles. J Hazard Mater **344:**749-757.

9. **Nancharaiah YV, Lens PN.** 2015. Selenium biomineralization for biotechnological applications. Trends Biotechnol **33:**323-330.

10. **Prasad G.** 2009. Biomedical applications of nanoparticles. In Safety of Nanoparticles, New York, NY, USA. Springer, pp. 89-109.

11. **Iranifam M, Fathinia M, Rad TS, Hanifehpour Y, Khataee A, Joo S.** 2013. A novel selenium nanoparticles-enhanced chemiluminescence system for determination of dinitrobutylphenol. Talanta **107:**263-269.

12. **Bai Y, Rong F, Wang H, Zhou Y, Xie X, Teng J.** 2011. Removal of copper from aqueous solutions by adsorption on elemental selenium nanoparticles. Journal of Chemical & Engineering Data **56:**2563-2568.

13. **Ramya S, Shanmugasundaram T, Balagurunathan R.** 2015. Biomedical potential of actinobacterially synthesized selenium nanoparticles with special reference to anti-biofilm, anti-oxidant, wound healing, cytotoxic and anti-viral activities. Journal of Trace Elements in Medicine and Biology **32:**30-39.

14. **Jain R, Dominic D, Jordan N, Rene ER, Weiss S, van Hullebusch ED, Hübner R, Lens PN.** 2016. Preferential adsorption of Cu in a multi-metal mixture onto biogenic elemental selenium nanoparticles. Chem Eng J **284:**917-925.

15. **Tian B, Van den Bossche J, Kostarelos K.** 2012. Design and engineering of multifunctional quantum dot-based nanoparticles for simultaneous therapeutic-diagnostic applications. In Svenson S, Prud'homme RK (eds) Multifunctional Nanoparticles for Drug Delivery Applications. Springer: New York, 2012; pp 345−365.

16. **Ren Y, Zhao T, Mao G, Zhang M, Li F, Zou Y, Yang L, Wu X.** 2013. Antitumor activity of hyaluronic acid–selenium nanoparticles in Heps tumor mice models. Int J Biol Macromol **57:**57-62.

17. **Wang J, Zhang Y, Yuan Y, Yue T.** 2014. Immunomodulatory of selenium nano-particles decorated by sulfated *Ganoderma lucidum* polysaccharides. Food and chemical toxicology **68:**183-189.

18. **Wang T, Yang L, Zhang B, Liu J.** 2010. Extracellular biosynthesis and transformation of selenium nanoparticles and application in H_2O_2 biosensor. Colloids and Surfaces B: Biointerfaces **80:**94-102.

19. **Tran PA, Webster TJ.** 2013. Antimicrobial selenium nanoparticle coatings on polymeric medical devices. Nanotechnology **24:**155101.

20. **Wadhwani SA, Shedbalkar UU, Singh R, Chopade BA.** 2016. Biogenic selenium nanoparticles: current status and future prospects. Appl Microbiol Biotechnol **100:**2555-2566.

21. **Oremland RS, Herbel MJ, Blum JS, Langley S, Beveridge TJ, Ajayan PM, Sutto T, Ellis AV, Curran S.** 2004. Structural and spectral features of selenium nanospheres produced by Se-respiring bacteria. Appl Environ Microbiol **70:**52-60.

22. **Xu H, Barton LL.** 2013. Se-bearing colloidal particles produced by sulfate-reducing bacteria and sulfide-oxidizing bacteria: TEM study. Advances in Microbiology **3:**205-211.

529 23. **Tugarova AV, Mamchenkova PV, Dyatlova YA, Kamnev AA.** 2017. FTIR and Raman
530 spectroscopic studies of selenium nanoparticles synthesised by the bacterium *Azospirillum*
531 *thiophilum*. Spectrochimica Acta Part A: Molecular and Biomolecular Spectroscopy **192:**458-
532 463.

533 24. **Ruiz-Fresneda M, Martín JD, Bolívar JG, Cantos MVF, Bosch-Estévez G, Moreno**
534 **MFM, Merroun ML.** 2018. Green synthesis and biotransformation of amorphous Se
535 nanospheres to trigonal 1D Se nanostructures: impact on Se mobility within the concept of
536 radioactive waste disposal. Environmental Science: Nano(5) **9:**2103-2116.

537 25. **Eswayah AS, Smith TJ, Scheinost AC, Hondow N, Gardiner PH.** 2017. Microbial
538 transformations of selenite by methane-oxidizing bacteria. Appl Microbiol Biotechnol
539 **101:**6713-6724.

540 26. **Chasteen TG.** 1993. Confusion between dimethyl selenenyl sulfide and dimethyl
541 selenone released by bacteria. Applied organometallic chemistry **7:**335-342.

542 27. **Burra R, Pradenas GA, Montes RA, Vásquez CC, Chasteen TG.** 2010. Production of
543 dimethyl triselenide and dimethyl diselenenyl sulfide in the headspace of metalloid-resistant
544 bacillus species grown in the presence of selenium oxyanions. Anal Biochem **396:**217-222.

545 28. **Dhanjal S, Cameotra SS.** 2010. Aerobic biogenesis of selenium nanospheres by Bacillus
546 cereus isolated from coalmine soil. Microbial cell factories **9:**52-62.

547 29. **Zhang L, Li D, Gao P.** 2012. Expulsion of selenium/protein nanoparticles through
548 vesicle-like structures by Saccharomyces cerevisiae under microaerophilic environment.
549 World Journal of Microbiology and Biotechnology **28:**3381-3386.

550 30. **Kamnev AA, Mamchenkova PV, Dyatlova YA, Tugarova AV.** 2017. FTIR
551 spectroscopic studies of selenite reduction by cells of the rhizobacterium Azospirillum
552 brasilense Sp7 and the formation of selenium nanoparticles. J Mol Struct **1140:**106-112.

553 31. **Meija J, Caruso JA.** 2004. Selenium and sulfur trichalcogenides from the chalcogenide
554 exchange reaction. Inorg Chem **43:**7486-7492.

555 32. **Vriens B, Mathis M, Winkel LH, Berg M.** 2015. Quantification of volatile-alkylated
556 selenium and sulfur in complex aqueous media using solid-phase microextraction. Journal of
557 Chromatography A **1407:**11-20.

558 33. **Scheinost AC, Charlet L.** 2008. Selenite reduction by mackinawite, magnetite and
559 siderite: XAS characterization of nanosized redox products. Environ Sci Technol **42:**1984-
560 1989.

561 34. **Scheinost AC, Kirsch R, Banerjee D, Fernandez-Martinez A, Zaenker H, Funke H,**
562 **Charlet L.** 2008. X-ray absorption and photoelectron spectroscopy investigation of selenite
563 reduction by FeII-bearing minerals. J Contam Hydrol **102:**228-245.

564 35. Vogel M, Fischer S, Maffert A, Hübner R, Scheinost AC, Franzen C Steudtner R. 2018.
565 Biotransformation and detoxification of selenite by microbial biogenesis of selenium-sulfur
566 nanoparticles. J. Hazard. Mater. **344:** 749-757.

567 36. **Naumann D, Keller S, Helm D, Schultz C, Schrader B.** 1995. FT-IR spectroscopy and
568 FT-Raman spectroscopy are powerful analytical tools for the non-invasive characterization of
569 intact microbial cells. J Mol Struct **347:**399-405.

570 37. **Alvarez-Ordonez A, Mouwen D, Lopez M, Prieto M.** 2011. Fourier transform infrared
571 spectroscopy as a tool to characterize molecular composition and stress response in
572 foodborne pathogenic bacteria. J Microbiol Methods **84:**369-378.

573 38. **Ojeda JJ, Dittrich M.** 2012. Fourier transform infrared spectroscopy for molecular
574 analysis of microbial, cells In: A. Navid (Ed.) Microbial Systems Biology: methods and
575 protocols (Methods in Molecular Biology, vol. 881), Chapter 8, Springer, New York, pp.
576 187-211.

577 39. **Beekes M, Lasch P, Naumann D.** 2007. Analytical applications of Fourier transform-
578 infrared (FT-IR) spectroscopy in microbiology and prion research. Vet Microbiol **123:**305-
579 319.

580 40. **Burattini E, Cavagna M, Dell'Anna R, Campeggi FM, Monti F, Rossi F, Torriani S.**
581 2008. A FTIR microspectroscopy study of autolysis in cells of the wine yeast Saccharomyces
582 cerevisiae. Vibrational Spectroscopy **47:**139-147.

583 41. **Kamnev AA.** 2008. FTIR spectroscopic studies of bacterial cellular responses to
584 environmental factors, plant-bacterial interactions and signalling. Journal of Spectroscopy
585 **22:**83-95.

586 42. **Shirsat S, Kadam A, Naushad M, Mane RS.** 2015. Selenium nanostructures: microbial
587 synthesis and applications. Rsc Advances **5:**92799-92811.

588 43. **Tugarova AV, Kamnev AA.** 2017. Proteins in microbial synthesis of selenium
589 nanoparticles. Talanta **174:**539-547.

590 44. **Naveau A, Monteil-Rivera F, Guillon E, Dumonceau J.** 2007. Interactions of aqueous
591 selenium (− II) and (IV) with metallic sulfide surfaces. Environ Sci Technol **41:**5376-5382.

592 45. **Lucovsky G, Mooradian A, Taylor W, Wright G, Keezer R.** 1967. Identification of the
593 fundamental vibrational modes of trigonal, α-monoclinic and amorphous selenium. Solid
594 State Commun **5:**113-117.

595 46. **Demchenko PY, Gladyshevskii RE, Volkov SV, Yanko OG, Kharkova LB, Fokina**
596 **ZA, Fokin AA.** 2010. The first nonaselenium ring. Chemical Communications **46:**4520-
597 4522.

598 47. **Yannopoulos S, Andrikopoulos K.** 2004. Raman scattering study on structural and
599 dynamical features of noncrystalline selenium. J Chem Phys **121:**4747-4758.

600 48. **Carini G, Cutroni M, Fontana M, Galli G, Migliardo P.** 1980. Resonant Raman
601 scattering in amorphous bulk selenium. Solid State Commun **33:**1143-1145.

49. **Baganich A, Mikla V, Semak D, Sokolov A, Shebanin A.** 1991. Raman scattering in amorphous selenium molecular structure and photoinduced crystallization. physica status solidi (b) **166:**297-302.

50. **Nagels P, Sleeckx E, Callaerts R, Tichy L.** 1995. Structural and optical properties of amorphous selenium prepared by plasma-enhanced CVD. Solid State Commun **94:**49-52.

51. **Machado K, Dubiel A, Deflon E, Kostrzepa I, Stolf S, Sanchez D, Jóvári P.** 2010. Investigation on vibrational and structural properties of amorphous Se1− xSx alloys produced by mechanical alloying by Raman spectroscopy, X-ray diffraction, EXAFS and RMC simulations. Solid State Commun **150:**1359-1363.

52. **Eysel H, Sunder S.** 1979. Homonuclear bonds in sulfur-selenium mixed crystals: a Raman spectroscopic study. Inorg Chem **18:**2626-2627.

53. **Kasuya A, Watanabe K, Takahashi H, Toji K, Motomiya K, Nishina Y.** 1996. Stability of SxSey ring clusters studied by Raman scattering. Materials Science and Engineering: A **217:**12-14.

54. **Kobayashi K, Tukada H, Kikuchi K, Ikemoto I.** 1986. NMR and XPS studies of some diselenocarbamates. Bond switch in bis (dimethylselenocarbamoyl) triselenide. Bull Chem Soc Jpn **59:**1741-1746.

55. **Dáaz F, Godoy A, Tagle L, Valdebenito N, Bernede J.** 1996. Poly (p-phenylene-diselenocarbonate) and poly (p-phenylene-diselenothiocarbonate): New semiconducting polymers. European polymer journal **32:**1155-1160.

56. **Ganther HE.** 1968. Selenotrisulfides. Formation by the reaction of thiols with selenious acid. Biochemistry (N Y) **7:**2898-2905.

57. **Ganther HE.** 1971. Reduction of the selenotrisulfide derivative of glutathione to a persulfide analog by gluthathione reductase. Biochemistry (N Y) **10:**4089-4098.

58. **Lampis S, Zonaro E, Bertolini C, Cecconi D, Monti F, Micaroni M, Turner RJ, Butler CS, Vallini G.** 2017. Selenite biotransformation and detoxification by Stenotrophomonas maltophilia SeITE02: novel clues on the route to bacterial biogenesis of selenium nanoparticles. J Hazard Mater **324:**3-14.

59. **Ward N, Larsen Ø, Sakwa J, Bruseth L, Khouri H, Durkin AS, Dimitrov G, Jiang L, Scanlan D, Kang KH.** 2004. Genomic insights into methanotrophy: the complete genome sequence of Methylococcus capsulatus (Bath). PLoS biology **2:**e303.

60. **Laitinen RS, Pekonen P, Suontamo RJ.** 1994. Homo-and heteroatomic chalcogen rings. Coord Chem Rev **130:**1-62.

61. **Jain R, Jordan N, Weiss S, Foerstendorf H, Heim K, Kacker R, Hübner R, Kramer H, Van Hullebusch ED, Farges F.** 2015. Extracellular polymeric substances govern the surface charge of biogenic elemental selenium nanoparticles. Environ Sci Technol **49:**1713-1720.

639 62. **Steudel R.** 1986. Hypervalent defects in amorphous selenium and similar lone-pair
640 semiconductors. J Non Cryst Solids **83:**63-79.

641 63. **Sonkusre P, Nanduri R, Gupta P, Cameotra SS.** 2014. Improved extraction of
642 intracellular biogenic selenium nanoparticles and their specificity for cancer
643 chemoprevention. Journal of Nanomedicine & Nanotechnology **5:**1-9.

644

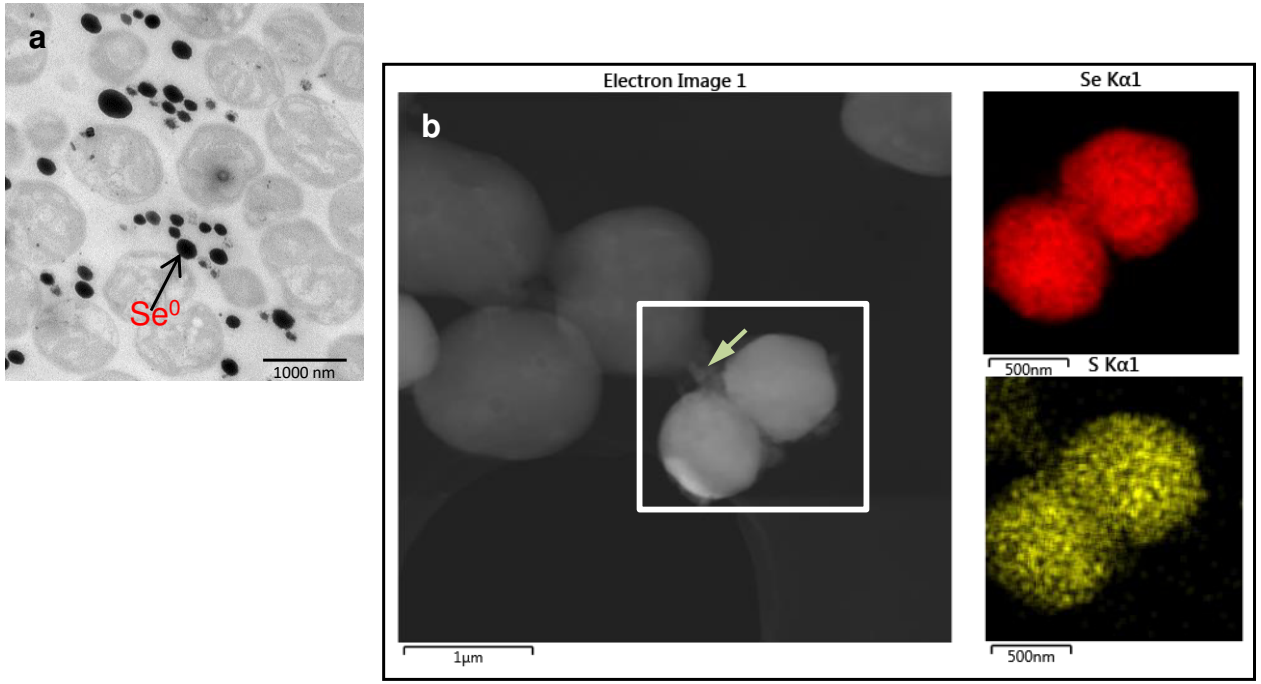
a
Se0
1000 nm
Electron Image 1
b
1µm
Se Kα1
500nm
S Kα1
500nm
c
Se0
200 nm
Intensity (arbitrary units)
Energy (keV)
Se
Cu
C
S
Cu
Se
Se
0
2
4
6
8
10
12
14

Figure2

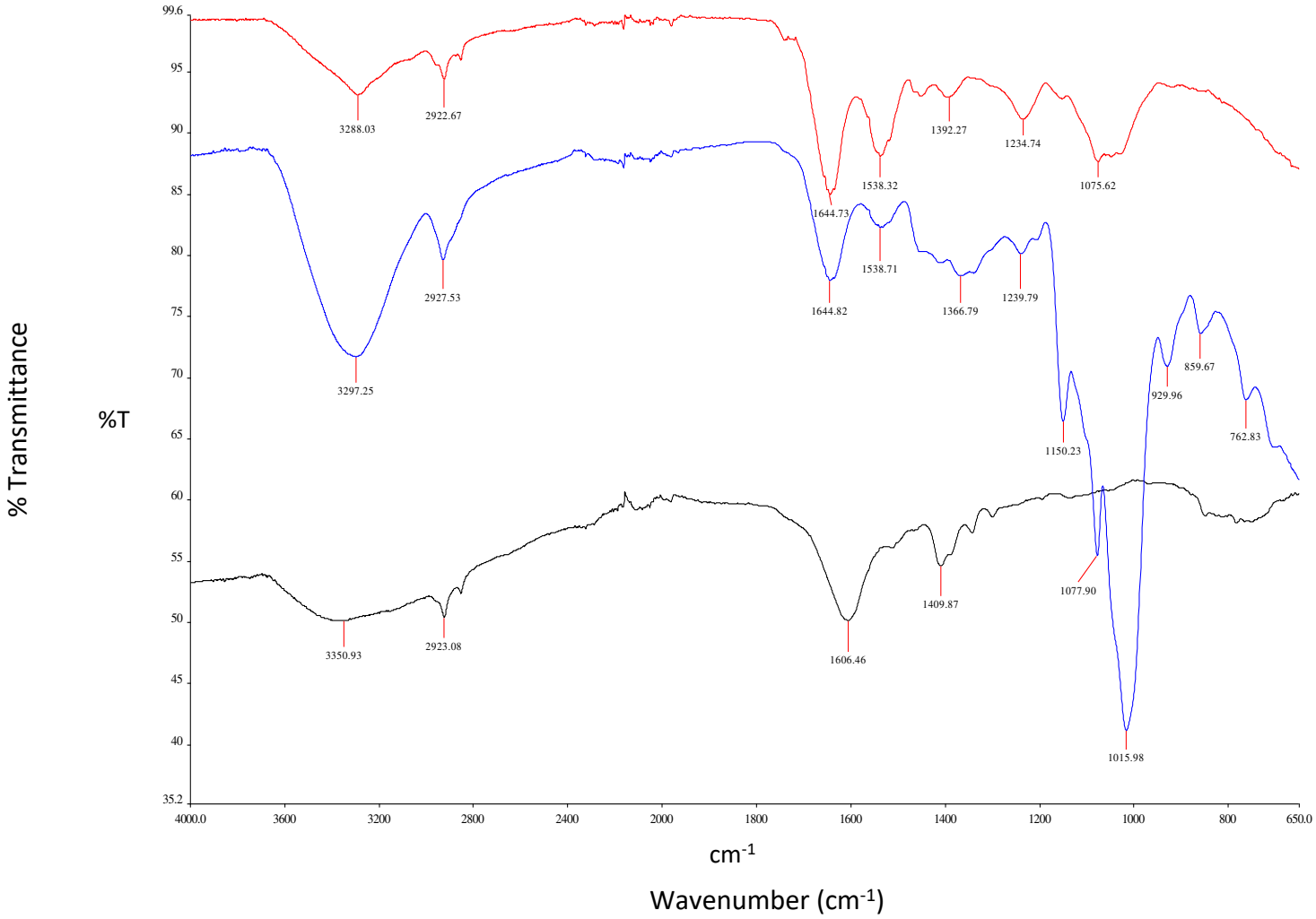
% Transmittance
%T
99.6
95
90
85
80
75
70
65
60
55
50
45
40
35.2
3288.03
2922.67
1644.73
1538.32
1392.27
1234.74
1075.62
3297.25
2927.53
1644.82
1538.71
1366.79
1239.79
1150.23
929.96
859.67
762.83
3350.93
2923.08
1606.46
1409.87
1077.90
1015.98
4000.0
3600
3200
2800
2400
2000
1800
1600
1400
1200
1000
800
650.0
cm-1
Wavenumber (cm-1)

Figure 3

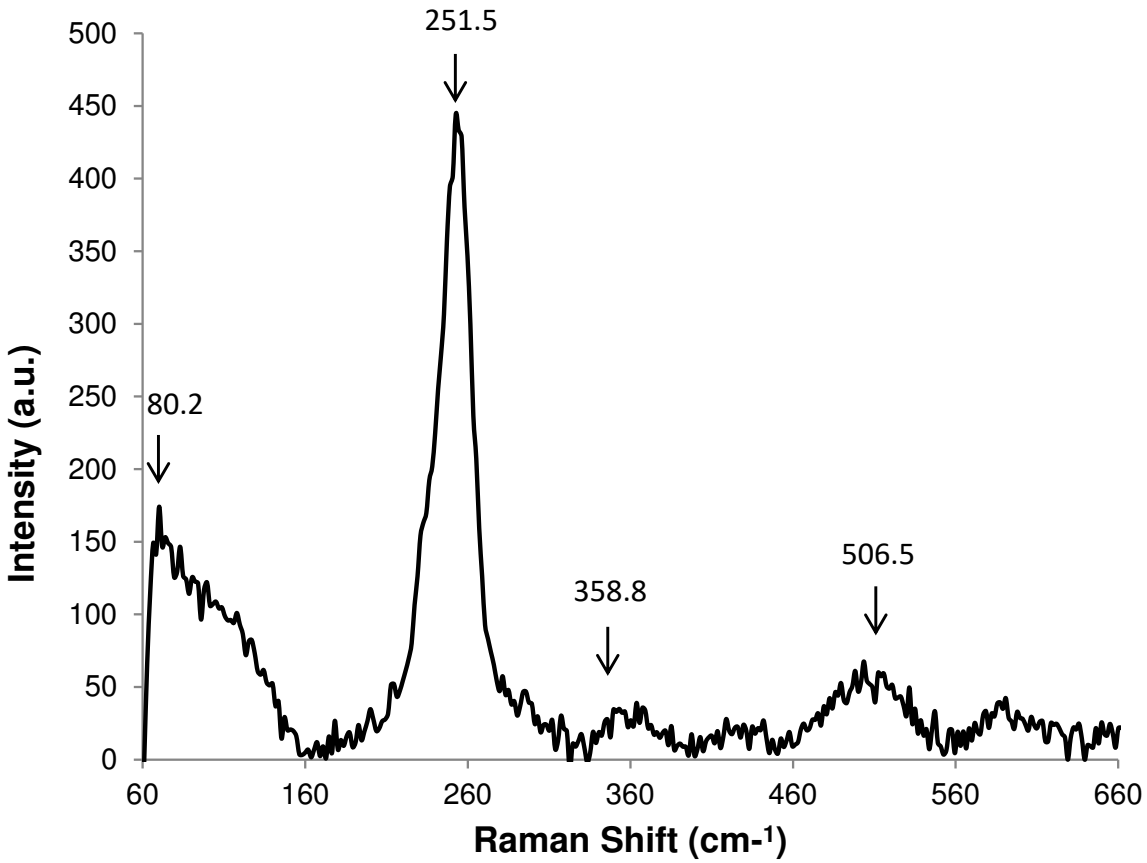
251.5
80.2
358.8
506.5
Intensity (a.u.)
Raman Shift (cm-1)
0
50
100
150
200
250
300
350
400
450
500
60
160
260
360
460
560
660

Figure 4

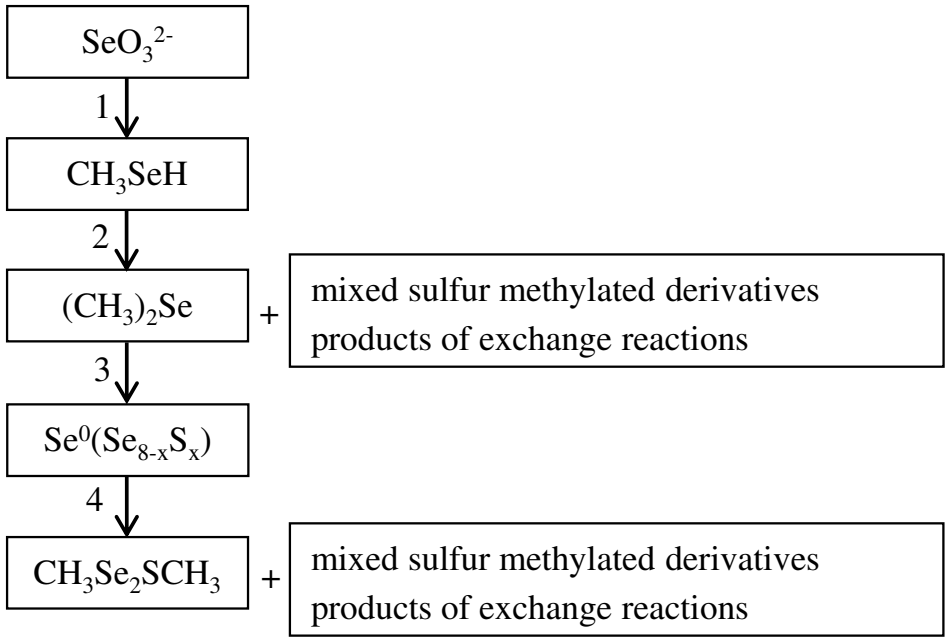
SeO_3^{2-}
1
CH_3SeH
2
$(CH_3)_2Se$
+
mixed sulfur methylated derivatives
products of exchange reactions
3
$Se^0(Se_{8-x}S_x)$
4
$CH_3Se_2SCH_3$
+
mixed sulfur methylated derivatives
products of exchange reactions

Figure 5

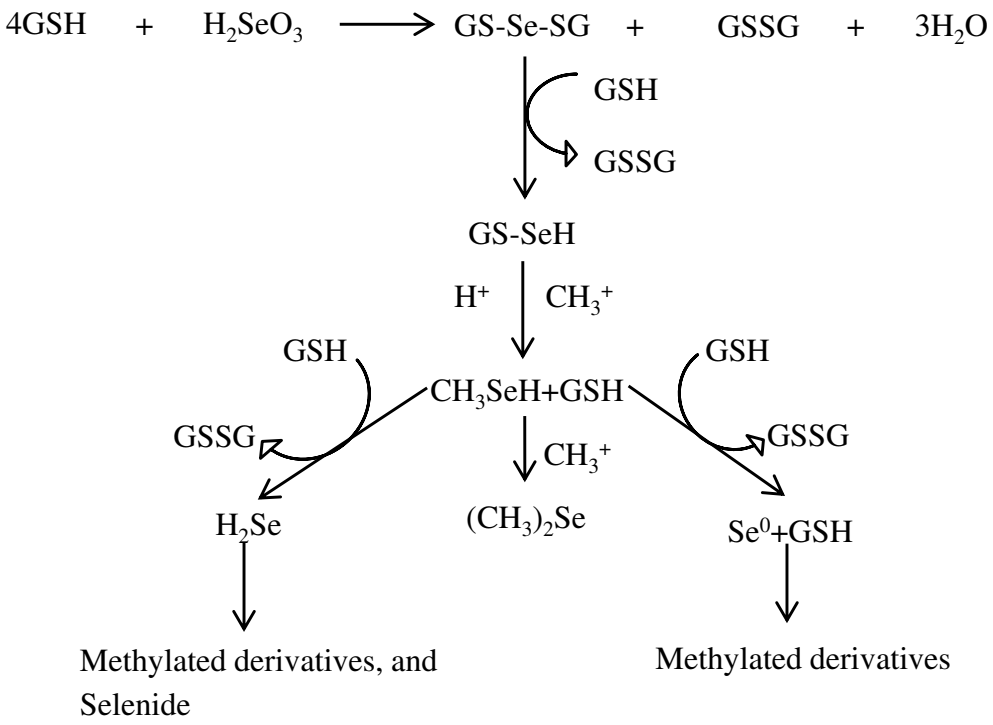
4GSH + H_2SeO_3 → GS-Se-SG + GSSG + $3H_2O$
GSH
GSSG
GS-SeH
H^+
CH_3^+
GSH
GSH
CH_3SeH+GSH
GSSG
GSSG
CH_3^+
H_2Se
$(CH_3)_2Se$
Se^0+GSH
Methylated derivatives, and Selenide
Methylated derivatives

List of Figures

Figure 1 TEM thin-section micrographs of *Mc. capsulatus* (a) exposed to 20 mg L^{-1} SeO_3^{2-}, showing the extracellular locations of the Se^0 nanospheres, HAADF-STEM imaging, showing Se nanospheres associated with the cells with EDX maps (generated from spectra collected from the indicated areas) of Se and S(b) and TEM of *Mc. capsulatus* cultures exposed to 20 mg L^{-1} SeO_3^{2-} (c) with EDX analysis within the electron dense regions (Se^0 nanospheres). The green arrow in part (b) indicates the "trail" of sulfur-containing material between the cells and the particles which may indicate partly particle-associated proteinaceous material derived from the cells. Cells were fixed with 3% glutaraldehyde and 2% OsO_4 immediately before the analysis.

Figure 2 The FTIR spectra of freeze dried Bio-SeNPs (blue) and bacterial biomass (red) of *Mc. capsulatus* exposed to 20 mg L^{-1} SeO_3^{2-} and harvested at OD_{600} ~ 0.7, separated by centrifugation, washed with phosphate buffered saline pH 7.2 and freeze dried; as well as Chem-SeNPs (black) obtained through reaction of Na_2SeO_3 with L-cysteine. The spectra are representatives of 5 runs of the experiments.

Figure 3 The Raman spectra of purified Se nanospheres from *Mc. capsulatus*

Figure 4 A schematic diagram showing the reduction of selenite to methyl selenol with the subsequent formation of other selenium-containing species. The numbers donate the following: 1. reduction & methylation, 2. reduction & methylation, 3. polymerization, 4. exchange reactions.

Figure 5 A schematic diagram showing the formation of methyl selenol, selenium particles and methylated derivatives.

List of Tables

Table 1 Tentative assignments of main bands to the relevant functional groups (wavenumber, cm^{-1}) (Naumann *et al.*, 1995; Beekes *et al.*, 2007; Burattini *et al.*, 2008; Kamnev, 2008; Alvarez-Ordonez *et al.*, 2011; Ojeda & Dittrich, 2012; Kamnev *et al.*, 2017).

Sample	O—H; N—H (amide A in proteins)	C—H in $>CH_2$)	C=O (ester moiety)	Amide I (in proteins)	Carboxyl COO^-)	Amide II (in proteins)	$-CH_2$/$-CH_3$ (in proteins, lipids, polyesters, etc.)	C=O of COO^-)	C—O—C/C—C—O (in ester moieties)	Amide III / O-P=O	C-O, C—C , C—H, C—O—C in polysaccharides, and	Phosphoryl groups	"fingerprint region"
Cell biomass of *Mc. capsulatus*	3288	2922		1644		1538		1392		1234	1075		
SeNPs produced by *Mc. capsulatus*	3297	2927		1644		1538		1366		1239	1150	919	859
											1077		762
											1015		
Chem-SeNPs		2923			1606			1409					

Table 2. A summary of the selenium- and sulfur-containing species detected in the headspace and solution after 4h and 20h incubation of *Mc. capsulatus* (Bath) in selenite amended medium using sorptive extraction in conjunction TD-GC-MS analysis. The control is the same medium with no added selenite.

Incubation Time		Species										
		Methyl selenol	DMSeS	DMDSe	Bis (Methylseleno) methane	Dimethyl selenosulfide	Dimethyl diselenenyl sulfide	Triselenothone/ Dimethyltriselenide	Benzothiazole	Diethyl sulfuxide	Propanesulfonyl	Dodecanethiol
In solution (selenite amended)	4 h	+	+	+	+	-	+	-	+	-	-	-
	20 h	+	+	+	+	+	+	+	+	+	-	-
In headspace (selenite amended)	4 h	+	+	+	-	-	-	-	+	-	-	-
	20 h	+	+	+	-	-	-	+	+	-	-	-
(Control)	20 h	-	-	-	-	-	-	-	+	-	+	+

The signs denote detected (+) and undetected (-).